Contents lists available at ScienceDirect

Physics Letters B

www.elsevier.com/locate/physletb

Exclusive production of $\rho^0\rho^0$ pairs in $\gamma\gamma$ collisions at RHIC

M. Kłusek [a,b], W. Schäfer [b,*], A. Szczurek [a,b]

[a] *University of Rzeszów, PL-35-959 Rzeszów, Poland*
[b] *Institute of Nuclear Physics PAN, PL-31-342 Cracow, Poland*

A R T I C L E   I N F O

A B S T R A C T

We discuss exclusive electromagnetic production of two neutral ρ mesons in coherent photon–photon processes in ultrarelativistic heavy-ion collisions. The cross section is calculated in the equivalent photon approximation (EPA). Both uncertainties of the flux factors and photon–photon cross sections are discussed in detail. We show that inclusion of precise charge densities in nuclei is essential for realistic evaluations of the nuclear photon–photon cross sections. We find that the cross section, especially with realistic flux factors, is sensitive to low energy in the subsystem $\gamma\gamma \to \rho^0\rho^0$. The experimental data for the $\gamma\gamma \to \rho^0\rho^0$ cross section extracted from e^+e^- collisions are parametrized and used to estimate the nucleus–nucleus cross section. In addition, we include vector-dominance-model (VDM)–Regge contribution which becomes important at large photon–photon energy. Large nuclear cross sections are obtained. We discuss a possibility of focusing on the large-energy component. We find that both ρ^0 mesons are produced predominantly at midrapidities and could be measured by the STAR Collaboration at RHIC.

© 2009 Elsevier B.V. Open access under CC BY license.

1. Introduction

Exclusive production of elementary particles (lepton pairs, Higgs, etc.) or mesons (vector mesons, pair of pseudoscalar mesons, etc.) in ultrarelativistic heavy-ion collisions is an interesting and quickly growing field [1–3] of theoretical investigation. On the experimental side the situation is slightly different. So far only the single-ρ^0 exclusive cross section $AA \to AA\rho^0$ was measured [4]. Here the dominant mechanism is the photoproduction described by the photon–Pomeron fusion.

In the present Letter we consider exclusive production of $\rho^0\rho^0$ pairs in $\gamma\gamma$ collisions. So far only the integrated cross section for $AA \to AA\rho^0\rho^0$ was roughly estimated in the literature [5,6], using a pQCD-inspired modelling of the Pomeron exchange between mesons for $AA \to AAJ/\Psi J/\Psi$ and $AA \to AA\rho^0 J/\Psi$ and assuming Regge factorization. Uncertainties of almost three-orders of magnitude were found. As we discuss here, in the $AA \to AA\rho^0\rho^0$ reaction one is sensitive rather to the close-to-threshold region for the $\gamma\gamma \to \rho^0\rho^0$ subprocess where the specific pQCD approaches of [6] are not applicable at all. Furthermore the Regge factorization for this hard and soft processes is likely broken. The $\rho^0\rho^0$ pair will eventually decay into the final state of four charged pions. If the $\rho^0\rho^0$ invariant mass is very large, the two $\pi^+\pi^-$-pairs will be separated by a large rapidity gap. It has been recently sug-gested that in this kinematics, charge asymmetries can be used to discover/study the QCD-Odderon exchange [7].

At the RHIC energies discussed here, we will be however dominated by $\gamma\gamma$ center-of-mass energies in the region of a few GeV. Here, experimental data for $\gamma\gamma \to \rho^0\rho^0$ are known and were measured by several groups at e^+e^- colliders [8]. Experimentally one observes a huge enhancement close to the threshold. The origin of this enhancement was never understood. Some speculations are discussed in Ref. [9]. The huge cross section at $W \approx 1.5$–2 GeV was interpreted as a tensor resonance decaying into $\rho^0\rho^0$ channel [10]. In Ref. [11] the Regge factorization was tested. In the following we shall see the consequences of the anomalous behaviour seen in the e^+e^- data for the two-photon production of the $\rho^0\rho^0$ pair in the nucleus–nucleus collisions.

2. Calculation

2.1. Equivalent photon approximation for nuclei

Let us consider the process $AA \to AA\rho^0\rho^0$ depicted in Fig. 1. The cross section takes the familiar form of a convolution of equivalent photon fluxes and $\gamma\gamma$-cross sections:

$$\frac{d\sigma(AA \to \rho^0\rho^0 AA; s_{AA})}{d^2\boldsymbol{b}}$$
$$= dn_{\gamma\gamma}(x_1, x_2, \boldsymbol{b})\,\hat{\sigma}(\gamma\gamma \to \rho^0\rho^0; x_1 x_2 s_{AA}) + \cdots. \quad (2.1)$$

* Corresponding author.
E-mail addresses: mariola.klusek@ifj.edu.pl (M. Kłusek),
wolfgang.schafer@ifj.edu.pl (W. Schäfer), antoni.szczurek@ifj.edu.pl (A. Szczurek).
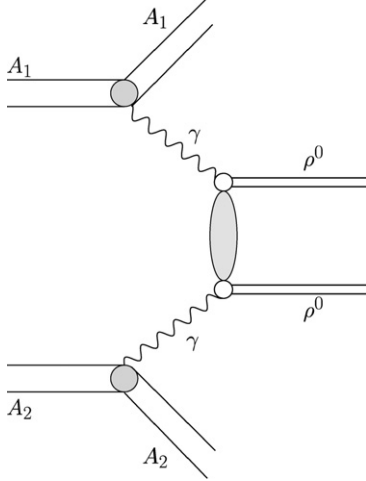
Fig. 1. The reaction discussed in this Letter.

Here we omitted helicity-dependent pieces, see below for more details. The effective photon flux is expressed through the electric field strengths of the ions and reads [12] (see also [13]):

$$dn_{\gamma\gamma}(x_1, x_2, \boldsymbol{b}) = \int d^2\boldsymbol{b}_1\, d^2\boldsymbol{b}_2\, S^2_{abs}(\boldsymbol{b})\delta^{(2)}(\boldsymbol{b} - \boldsymbol{b}_1 + \boldsymbol{b}_2)\frac{dx_1}{x_1}\frac{dx_2}{x_2}$$
$$\times \frac{1}{\pi^2}\big|\boldsymbol{E}(x_1, \boldsymbol{b}_1)\big|^2\big|\boldsymbol{E}(x_2, \boldsymbol{b}_2)\big|^2, \qquad (2.2)$$

where the electromagnetic field strengths are given in terms of the charge form factor of the nucleus $F_{em}(\vec{q}^2)$ by:

$$\boldsymbol{E}(x, \boldsymbol{b})$$
$$= Z\sqrt{4\pi\alpha_{em}} \int \frac{d^2\boldsymbol{q}}{(2\pi)^2} \exp[-i\boldsymbol{b}\boldsymbol{q}]\frac{\boldsymbol{q}}{\boldsymbol{q}^2 + x^2 M_A^2} F_{em}(\boldsymbol{q}^2 + x^2 M_A^2)$$
$$= -iZ\sqrt{4\pi\alpha_{em}}\frac{\boldsymbol{b}}{b^2}\int \frac{dq^2}{4\pi}\frac{(bq)J_1(bq)}{\boldsymbol{q}^2 + x^2 M_A^2}F_{em}(\boldsymbol{q}^2 + x^2 M_A^2). \qquad (2.3)$$

In practice $F_{em}(\vec{q}^2)$ is obtained as the Fourier transform of the nuclear charge densities extracted from electron–nucleus scattering data, for a useful compilation, see [14,15]. By putting $F_{em} \equiv 1$ one obtains the well-known result for a point-like charge (see e.g. the textbook [16]):

$$\boldsymbol{E}_{pt}(x, \boldsymbol{b}) = -i\frac{Z\sqrt{4\pi\alpha_{em}}}{2\pi}\frac{\boldsymbol{b}}{b^2}(xM_Ab)K_1(xM_Ab). \qquad (2.4)$$

Notice that our formula for the effective Weizsäcker–Williams flux of photons includes the impact-parameter dependent absorption factor $S^2_{abs}(\boldsymbol{b})$. It represents the probability that no inelastic interaction between the nuclei occurs. At RHIC energies it could be for example estimated from Glauber theory using the Czyż–Maximon [17] approximation:

$$S^2_{abs}(\boldsymbol{b}) = \exp\left(-\sigma_{NN}^{tot}\int d^2\boldsymbol{s}\, T_A(\boldsymbol{b} - \boldsymbol{s})T_A(\boldsymbol{s})\right), \qquad (2.5)$$

where $T_A(\boldsymbol{b})$ is the optical thickness of the nucleus. We checked, that for our purposes it can be well approximated by the result for black disc nuclei:

$$S^2_{abs}(\boldsymbol{b}) = \theta(b - 2R_A). \qquad (2.6)$$

The presence of the absorption factor also induces an azimuthal correlation between impact parameters $\boldsymbol{b}_1$ and $\boldsymbol{b}_2$. Now, soft photons are polarized linearly in the transverse plane, and therefore a subtle helicity dependence arises. Strictly speaking, one should write

$$\frac{d\sigma(AA \to \rho^0\rho^0 AA; s_{AA})}{d^2\boldsymbol{b}} = dn_{\gamma\gamma}^{\parallel}(x_1, x_2, \boldsymbol{b})\hat{\sigma}_{\parallel}(\gamma\gamma \to \rho^0\rho^0)$$
$$+ dn_{\gamma\gamma}^{\perp}(x_1, x_2, \boldsymbol{b})\hat{\sigma}_{\perp}(\gamma\gamma \to \rho^0\rho^0), \qquad (2.7)$$

where

$$dn_{\gamma\gamma}^{\parallel}(x_1, x_2, \boldsymbol{b}) = \int d^2\boldsymbol{b}_1\, d^2\boldsymbol{b}_2\, S^2_{abs}(\boldsymbol{b})\delta^{(2)}(\boldsymbol{b} - \boldsymbol{b}_1 + \boldsymbol{b}_2)\frac{dx_1}{x_1}\frac{dx_2}{x_2}\frac{1}{\pi^2}$$
$$\times \big|\boldsymbol{E}(x_1, \boldsymbol{b}_1) \cdot \boldsymbol{E}(x_2, \boldsymbol{b}_2)\big|^2,$$

$$dn_{\gamma\gamma}^{\perp}(x_1, x_2, \boldsymbol{b}) = \int d^2\boldsymbol{b}_1\, d^2\boldsymbol{b}_2\, S^2_{abs}(\boldsymbol{b})\delta^{(2)}(\boldsymbol{b} - \boldsymbol{b}_1 + \boldsymbol{b}_2)\frac{dx_1}{x_1}\frac{dx_2}{x_2}\frac{1}{\pi^2}$$
$$\times \big|\big[\boldsymbol{E}(x_1, \boldsymbol{b}_1) \times \boldsymbol{E}(x_2, \boldsymbol{b}_2)\big]\big|^2, \qquad (2.8)$$

are the fluxes for photons with parallel ($\parallel$), and perpendicular ($\perp$) linear polarizations; $\sigma^{\parallel}$ and $\sigma^{\perp}$ are the corresponding $\gamma\gamma$ cross sections. The small effects associated with this helicity dependence have been discussed in [12] and will be neglected here.

A further comment on the practical uses of the equivalent photon approximation is in order. It is often pointed out that the Fermi–Weizsäcker–Williams idea of the equivalent photon flux represents indeed the archetypical parton-model concept. In this spirit, often flux factors of equivalent photons are calculated as for point-like particles with charge Ze, and the total cross section is then evaluated using a simple parton-model type formula:

$$\sigma(AA \to A(\rho^0\rho^0)A) = \int d\omega_1\, d\omega_2 \frac{n(\omega_1)}{\omega_1}\frac{n(\omega_2)}{\omega_2}\hat{\sigma}(\gamma\gamma \to \rho^0\rho^0). \qquad (2.9)$$

When calculating the two-dimensional integral it must be checked if $W^2 = 4\omega_1\omega_2 > 4m_\rho^2$. Here

$$n(\omega) \equiv \int d^2\boldsymbol{b}\, N(\omega, \boldsymbol{b}) = \frac{1}{\pi}\int d^2\boldsymbol{b}\big|\boldsymbol{E}(x, \boldsymbol{b})\big|^2, \quad x = \frac{\omega}{\gamma M_A}, \qquad (2.10)$$

is the flux of photons in an ultrarelativistic charge of energy γM_A. For RHIC, at the cms-energy $\sqrt{s_{NN}} = 200$ GeV we have $\gamma \sim 100$.

Notice that such a factorized form is not borne out by the general formula (2.2) which accounts for the strong absorptive corrections. One cannot meaningfully improve the b-integrated Eq. (2.9) to effectively account for strong absorption, in particular this is *not* achieved by simply restricting the impact parameter integrals (2.10) of the individual photon fluxes.

When written in terms of photon energies ω_i in the nucleus–nucleus center-of-mass, formula (2.1) takes the well-known form [12]

$$\sigma(AA \to A(\rho^0\rho^0)A; s_{AA})$$
$$= \int d^2\boldsymbol{b}_1\, d^2\boldsymbol{b}_2\, \theta(|\boldsymbol{b}_1 - \boldsymbol{b}_2| - 2R_A)\frac{d\omega_1}{\omega_1}\frac{d\omega_2}{\omega_2}N(\omega_1, \boldsymbol{b}_1)N(\omega_2, \boldsymbol{b}_2)$$
$$\times \hat{\sigma}(\gamma\gamma \to \rho^0\rho^0; 4\omega_1\omega_2). \qquad (2.11)$$

We also use the $\gamma\gamma$ cms-energy $W_{\gamma\gamma}$, and the rapidity-type variable Y defined through

$$\omega_1 = \frac{W_{\gamma\gamma}}{2}e^Y, \qquad \omega_2 = \frac{W_{\gamma\gamma}}{2}e^{-Y},$$
$$\frac{d\omega_1}{\omega_1}\frac{d\omega_2}{\omega_2} = 2\frac{dW_{\gamma\gamma}}{W_{\gamma\gamma}}dY. \qquad (2.12)$$

The $\sigma(\gamma\gamma \to \rho^0\rho^0)$ cross section can be calculated from models and/or taken from experimental data, if existing. Below we discuss separately the low-$W_{\gamma\gamma}$ and high-$W_{\gamma\gamma}$ case.
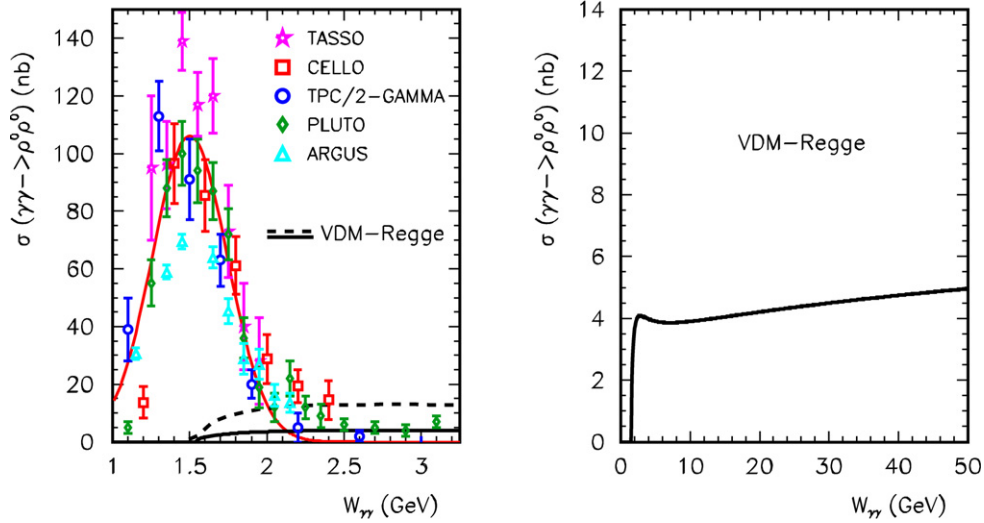
Fig. 2. The elementary cross section for the $\gamma\gamma \to \rho^0\rho^0$ reaction. In the left panel we display the collection of the e^+e^- experimental data [8,18] and our fit. In the right panel we show our predictions based on the VDM–Regge model described in the text. For comparison we show by the dashed line in the left panel also the result when the form factor correcting for off-shell effect is ignored.

2.2. Low-energy $\gamma\gamma \to \rho^0\rho^0$ cross section

The cross section for this process was measured up to $W_{\gamma\gamma} = 4$ GeV [18]. At low energy one observes a huge increase of the cross section. Several possible scenarios were discussed in this context (see e.g. Ref. [9]). For one real and one virtual photon induced processes the enhancement was interpreted as due to an isotensor meson decay [10]. We leave the difficult problem of the microscopic origin of the close-to-threshold bump for future studies and take here a pragmatic attitude of using directly experimental data.

In Fig. 2 we have collected the world data (see [8,18] and references therein). A huge rise of the cross section can be seen close to the threshold. Here we shall use rather directly experimental data in order to evaluate the cross section in nucleus–nucleus collisions. In Fig. 2 we show our fit to the world data. One can observe a small inconsistency of the data measured by different groups. This means that also our parametrization has about 20% accuracy.

2.3. High-energy $\gamma\gamma \to \rho^0\rho^0$ cross section

The cross section above $W_{\gamma\gamma} = 4$ GeV was never measured in the past. It is well known that the cross section for $\gamma\gamma \to$ hadrons can be well described in the VDM–Regge type model. Here we present a similar approach but for the specific, well defined, final state channel $\rho^0\rho^0$.

In the VDM–Regge approach the amplitude for the $\gamma\gamma \to \rho^0\rho^0$ can be written as

$$\mathcal{M}_{\gamma\gamma \to \rho^0\rho^0}(\hat{s}, \hat{t}; q_1, q_2) = C_{\gamma \to \rho^0} C_{\gamma \to \rho^0} \mathcal{M}_{\rho^{0*}\rho^{0*} \to \rho^0\rho^0}(\hat{s}, \hat{t}; q_1, q_2).$$
(2.13)

Above $C_{\gamma \to \rho^0} = \sqrt{f_\rho^2}$ and we use $f_\rho^2 = \frac{\alpha_{em}^2}{2.54}$. The later value is obtained in order to reproduce the decay width of the ρ^0 meson into dileptons.

For energies $W_{\gamma\gamma} > 2$–3 GeV the amplitude for the $\rho^{0*}\rho^{0*} \to \rho^0\rho^0$ processes can be written in the Regge form[1]:

$$\mathcal{M}_{\rho^{0*}\rho^{0*} \to \rho^0\rho^0}(\hat{s}, \hat{t}) = \hat{s}\left(\eta_{\mathbb{P}}(\hat{s}, \hat{t}) C_{\mathbb{P}} \left(\frac{\hat{s}}{s_0} \right)^{\alpha_{\mathbb{P}}(\hat{t})-1} \right.$$
$$\left. + \eta_{\mathbb{R}}(\hat{s}, \hat{t}) C_{\mathbb{R}} \left(\frac{\hat{s}}{s_0} \right)^{\alpha_{\mathbb{R}}(\hat{t})-1} \right) \cdot F(\hat{t}; q_1^2) F(\hat{t}; q_2^2).$$
(2.14)

Above we have introduced vertex form factors which, in general, are functions of exchanged Pomeron/Reggeon four-momentum and photon (ρ^0 meson) virtualities. We parametrize them in the factorized form:

$$F(\hat{t}; q^2) = \exp\left(\frac{B\hat{t}}{4} \right) \cdot \exp\left(\frac{q^2 - m_\rho^2}{2\Lambda^2} \right).$$
(2.15)

The second term, which "corrects" for ρ^0 meson virtuality, is normalized to unity when ρ^0 meson is on mass shell. We expect the slope parameter of the order $B \sim 4$ GeV^{-2} and the parameter responsible for off-shellness of ρ^0 mesons $\Lambda \sim 1$ GeV. We take the powers of the Pomeron ($\alpha_{\mathbb{P}}$) and Reggeon ($\alpha_{\mathbb{R}}$) terms from the Donnachie–Landshoff fit to the total NN and πN cross sections [19]. The parameters $C_{\mathbb{P}}$ and $C_{\mathbb{R}}$ are obtained assuming Regge factorization and assuming that $\sigma(\rho^0\rho^0 \to \rho^0\rho^0) = \sigma(\pi^0\pi^0 \to \pi^0\pi^0)$ (see e.g. [20], they are: $C_{\mathbb{P}} = 8.56$ mb, $C_{\mathbb{R}} = 13.39$ mb). While this seems justified for the Pomeron term, it is not so obvious if it is true for the Reggeon terms. Consistent with our choice of normalization $\eta_{\mathbb{P}}(\hat{s}, \hat{t})$ and $\eta_{\mathbb{R}}(\hat{s}, \hat{t})$ are complex functions such that: $\eta_{\mathbb{P}}(\hat{s}, \hat{t} = 0) \approx i$ and $\eta_{\mathbb{R}}(\hat{s}, \hat{t} = 0) \approx i - 1$. Standard signature functions [21] are normalized somewhat differently. The Pomeron and Reggeon trajectories are parametrized as $\alpha_{\mathbb{P}}(t) = 1.088 + 0.25t$ and $\alpha_{\mathbb{R}}(t) = 0.5 + 0.9t$.

The differential cross section can be obtained from the corresponding amplitude as:

$$\frac{d\sigma_{\gamma\gamma \to \rho^0\rho^0}}{d\hat{t}} = \frac{1}{16\pi\hat{s}^2} |\mathcal{M}_{\gamma\gamma \to \rho^0\rho^0}|^2.$$
(2.16)

The total cross section $\hat{\sigma}$ can be obtained by integrating (2.16) over $\hat{t}$

$$\hat{\sigma}_{\gamma\gamma \to \rho^0\rho^0} = \int_{t_{\min}(\hat{s})}^{t_{\max}(\hat{s})} \frac{d\hat{\sigma}}{d\hat{t}} d\hat{t},$$
(2.17)

where $t_{\min}$ and $t_{\max}$ are $\hat{s}$-dependent kinematical limitations of $\hat{t}$.

---

[1] We assume helicity conservation and neglect helicity flip in the present analysis. As far as only a good fit of the total cross section is concerned this is of no further relevance for our purposes.
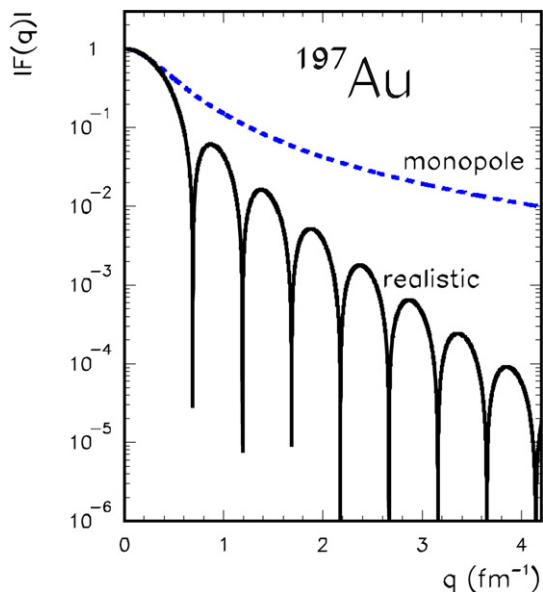
Fig. 3. The modulus of the charge form factor $F_{em}(q)$ of the ^{197}Au nucleus for realistic charge distribution (solid). For comparison we show the monopole form factor often used in practical applications (dashed).

Fig. 4. The $Au + Au \rightarrow Au + Au + \rho^0\rho^0$ cross section as a function of $W_{\gamma\gamma} = M_{\rho\rho}$ for the RHIC energy $\sqrt{s_{NN}} = 200$ GeV.

In Fig. 2 we present the corresponding t-integrated cross section together with existing experimental data taken from [8,18]. Here the solid line includes the off-shell form factor while the dashed line does not. The vanishing of the VDM–Regge cross section at $W_{\gamma\gamma} = 2m_\rho$ is due to t_{min}, t_{max} limitations. It is obvious from Fig. 2 that the VDM–Regge model cannot explain the huge close-to-threshold enhancement. Up to now the origin of this enhancement remains unclear. The VDM–Regge model nicely describes the experimental data for $W_{\gamma\gamma} \gtrsim 2.5$ GeV.

3. Results

The main ingredient for the calculation of photon fluxes is the charge form factor of the nucleus. In Fig. 3 we show the charge form factor of ^{197}Au calculated from the realistic charge density as measured in electron scattering off nuclei [15]. One can observe many oscillations characteristic for relatively sharp edge of the nucleus. This form factor is used to calculate flux of equivalent photons according to Eqs. (2.2) and (2.3). To illustrate the sensitivity of our calculation on details of the form factor, we also show a monopole form factor adjusted to the correct charge radius of the nucleus $F_{ch}(\vec{q}^2) = \Lambda^2/(\Lambda^2 + \vec{q}^2)$, with $\Lambda = 83$ MeV.

In Fig. 4 we show the distribution of the cross section for the nucleus–nucleus scattering in photon–photon center-of-mass energy $W_{\gamma\gamma}$ for both the low-energy component and high-energy VDM–Regge component. Below $W_{\gamma\gamma} = 2$ GeV the low-energy component dominates. The situation reverses above $W_{\gamma\gamma} = 2$ GeV. To study the high energy component one must impose an extra cut on $W_{\gamma\gamma}$, that is, the $\rho\rho$ invariant mass $M_{\rho\rho}$. However, at RHIC energies the high-energy tail of the photon spectrum is small, and the nuclear cross section drops quickly with the increasing invariant mass of two-ρ mesons. By the solid lines we show the results for the realistic nuclear form factor, while the dashed lines refer to the monopole form factor. The results obtained with the different form factors start to diverge at $W_{\gamma\gamma} \gtrsim 4$ GeV. This is due to the increasing longitudinal momentum transfer involved for higher invariant mass of the produced system. The γ-factors at RHIC are not too large, so that the form-factor suppression is felt already at such moderate invariant masses. The result for the point-like nucleus is shown by the dotted line.
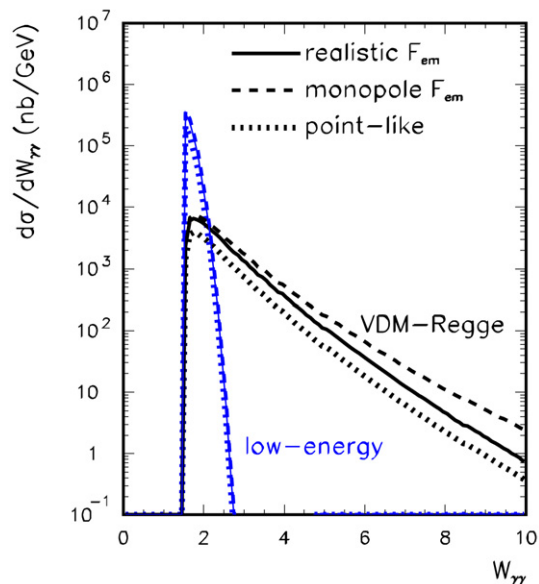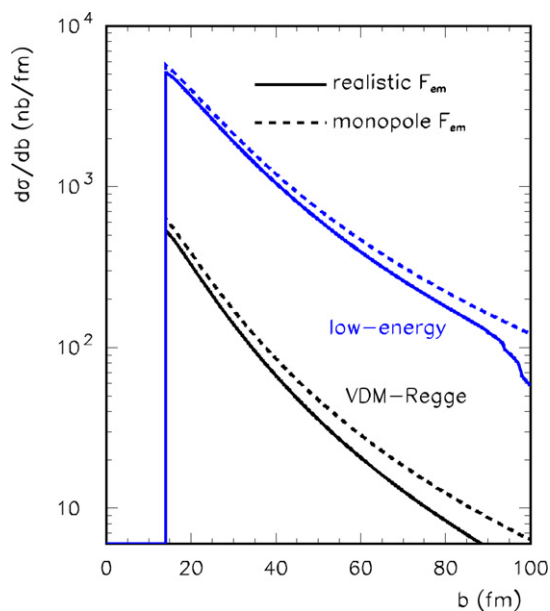

Fig. 5. The $Au + Au \rightarrow Au + Au + \rho^0\rho^0$ cross section as a function of the impact parameter b for $\sqrt{s_{NN}} = 200$ GeV.

In Fig. 5 we show the distribution in impact parameter $b = |\boldsymbol{b}_1 - \boldsymbol{b}_2|$ (see also Fig. 6). Again, we show distributions for the low- and high-energy components separately. Also shown are the distributions for the monopole form factor and for realistic charge density from [15]. One can clearly see different results for different approaches to calculate flux factors of equivalent photons. The sharp cutoff at $b = 2R_A \sim 14$ fm is precisely the θ-function coming from absorptive corrections.

Finally in Fig. 7 we show distribution in rapidity-like variable Y. As far as small invariant masses of $\rho^0\rho^0$ pairs dominate, we may refer to it as a rapidity of the $\rho^0\rho^0$ pair. Compared to the point-like case, the distribution obtained with realistic charge density is concentrated at midrapidities, and configurations when both ρ^0's are in very forward or both ρ^0's are in very backward directions are strongly damped compared to the case with point-like nucleus

charges. At larger rapidities, one can again see a substantial difference between results obtained with an approximate monopole form factor and with the exact one calculated from realistic charge density.

4. Conclusions

We have calculated, for the first time, realistic cross sections for exclusive $\rho^0\rho^0$ production in ultrarelativistic heavy-ion collisions at RHIC in the framework of equivalent photon approximation. We have discussed uncertainties related to the way how the nuclear photon flux is calculated. We have used realistic charge densities to calculate the nuclear charge form factors. The absorption effects have been included.

The low-energy part of the elementary $\gamma\gamma \to \rho^0\rho^0$ process has been parametrized and the parameters have been fitted to the e^+e^- data while the high-energy part has been modeled in the vector-dominance Regge type model with parameters which are used to describe other hadronic processes. The model turned out to be consistent with the highest-energy data points ($W \sim$ 3–4 GeV) from e^+e^- collisions.

It was shown that a realistic calculation of both ingredients is necessary to make reliable estimates of the nucleus–nucleus exclusive production of the $\rho^0\rho^0$ pairs. Large cross sections, of the order of fraction of milibarn, have been found. The bulk of the cross section is, however, concentrated in low photon–photon energies (low $\rho^0\rho^0$ invariant masses). Making cuts on higher $\rho^0\rho^0$ invariant masses one can easily select high-energy component. The ρ^0 mesons, decaying into $\pi^+\pi^-$, can be measured e.g. by the STAR

detector at RHIC. In fact preliminary data on coherently produced $\pi^+\pi^-\pi^+\pi^-$ have been shown in [22]. A Monte Carlo study is necessary to analyse feasibility of a measurement of the $\gamma\gamma$ process discussed here.

In particular a comment on competing production mechanisms is in order. Purely strong (Pomeron–Pomeron fusion) mechanisms suffer much stronger absorption and are hence suppressed for heavy nuclei (see for example the estimates for LHC energies in [23]). Coherent strong photonuclear reactions (the γ–Pomeron fusion) share a number of features with the coherent $\gamma\gamma$ processes, and can have comparable, or larger cross sections. In particular the four pion final state of relevance in this Letter could be populated through the coherent production $\gamma A \to \rho' A$ of higher excitations of the ρ-meson. Furthermore, as pointed out in Ref. [24] (see also [2] and references therein), at higher orders in photon exchanges there is a possibility of producing two ρ^0 mesons through the photonuclear mechanism.

Here we take the attitude that in principle photon exchanges stand out from all hadronic exchange mechanisms through the sharp forward peaks and very small transverse momentum transfers involved. The isolation of the contributions from $\gamma\gamma$ must therefore involve cuts on transverse momenta of the produced system and warrant further investigations on the detailed properties of the competing mechanisms.

In the present analysis we have concentrated on processes with final nuclei in the ground state. It is very difficult, if not impossible, to measure such very forward/backward nuclei. The multiple Coulomb excitations associated with $\rho^0\rho^0$ production may cause additional excitation of one or even both nuclei to the giant resonance region. The neutron emission from the giant resonances can be used then to tag the processes. The zero-degree calorimeters (ZDC) at RHIC can be used to measure such neutrons. We plan a detailed study of these processes in the future.
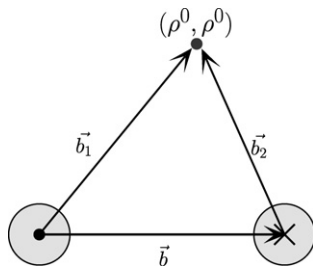
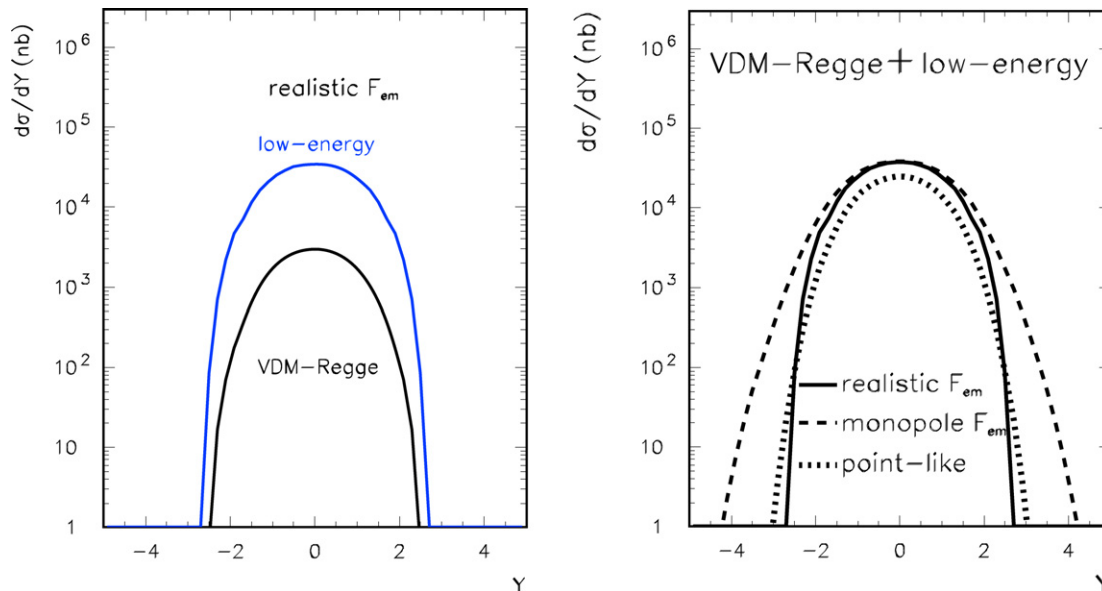**Fig. 6.** The quantities used in the impact parameter calculation.

Fig. 7. The Au + Au → Au + Au + $\rho^0\rho^0$ cross section as a function of the rapidity of the $\rho^0\rho^0$ pair Y for $\sqrt{s_{NN}} = 200$ GeV. In the left panel we show the decomposition into low- and high-energy contributions. The right panel shows the sensitivity to the nuclear form factor.

References

[1] V.M. Budnev, I.F. Ginzburg, G.V. Meledin, V.G. Serbo, Phys. Rep. 15 (1975) 181.
[2] G. Baur, K. Hencken, D. Trautmann, S. Sadovsky, Y. Kharlov, Phys. Rep. 364 (2002) 359.
[3] K. Hencken, et al., Phys. Rep. 458 (2008) 1.
[4] B.I. Abelev, et al., STAR Collaboration, Phys. Rev. C 77 (2008) 034910.
[5] S. Klein, E. Scannapieco, A talk at Photon 97, Egmond aan Zee, Netherlands, 10–15 May 1997, arXiv:hep-ph/9706358.
[6] V.P. Goncalves, M.V.T. Machado, Eur. Phys. J. C 29 (2003) 271;
    V.P. Goncalves, M.V.T. Machado, W.K. Sauter, Eur. Phys. J. C 46 (2006) 219.
[7] B. Pire, F. Schwennsen, L. Szymanowski, S. Wallon, Phys. Rev. D 78 (2008) 094009;
    B. Pire, F. Schwennsen, L. Szymanowski, S. Wallon, arXiv:0811.0255.
[8] M. Althoff, et al., TASSO Collaboration, Z. Phys. C 16 (1982) 13;
    H.J. Behrend, et al., CELLO Collaboration, Z. Phys. C 21 (1984) 205;
    H. Aihara, et al., TWO-GAMMA Collaboration, Phys. Rev. D 37 (1988) 28;
    Ch. Berger, et al., PLUTO Collaboration, Z. Phys. C 38 (1988) 521;
    H. Albrecht, et al., ARGUS Collaboration, Z. Phys. C 50 (1991) 1;
    P. Achard, et al., L3 Collaboration, Phys. Lett. B 568 (2003) 11.
[9] J.L. Rosner, Phys. Rev. D 70 (2004) 034028.
[10] I.V. Anikin, B. Pire, O.V. Teryaev, Phys. Lett. B 626 (2005) 86.
[11] G. Alexander, A. Levy, U. Maor, Z. Phys. C 30 (1986) 65.
[12] G. Baur, L.G. Ferreira Filho, Nucl. Phys. A 518 (1990) 786.
[13] R.N. Cahn, J.D. Jackson, Phys. Rev. D 42 (1990) 3690.
[14] R.C. Barrett, D.F. Jackson, Nuclear Sizes and Structure, Clarendon Press, Oxford, 1977.
[15] H. de Vries, C.W. de Jager, C. de Vries, At. Data Nucl. Data Tables 36 (1987) 495.
[16] J.D. Jackson, Classical Electrodynamics, 2nd ed., Wiley, New York, 1975, p. 722.
[17] W. Czyż, L.C. Maximon, Ann. Phys. 52 (1969) 59.
[18] D. Morgan, M.R. Pennington, M.R. Whalley, J. Phys. G 20 (8A) (1994) A1.
[19] A. Donnachie, P.V. Landshoff, Phys. Lett. B 296 (1992) 227.
[20] A. Szczurek, N.N. Nikolaev, J. Speth, Phys. Rev. C 66 (2002) 055206.
[21] S. Donnachie, G. Dosch, P. Landshoff, O. Nachtmann, Pomeron Physics and QCD, Cambridge Univ. Press, Cambridge, 2002.
[22] B. Grube, et al., STAR Collaboration, arXiv:0808.3991 [nucl-ex];
    S.R. Klein, arXiv:0810.3039 [nucl-ex].
[23] R. Engel, M.A. Braun, C. Pajares, J. Ranft, Z. Phys. C 74 (1997) 687.
[24] S. Klein, J. Nystrand, Phys. Rev. C 60 (1999) 014903.